Computers and Mathematics with Applications 60 (2010) 1135–1144

Contents lists available at ScienceDirect

Computers and Mathematics with Applications

journal homepage: www.elsevier.com/locate/camwa

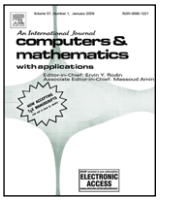

On the finite-volume Lattice Boltzmann modeling of thermo-hydrodynamics

J. Ghasemi [a,*], S.E. Razavi [b]

[a] Faculty of Engineering, Zanjan University, Zanjan, 45195-313, Iran
[b] Faculty of Mechanical Engineering, Tabriz University, Tabriz, Iran

ARTICLE INFO

Article history:
Received 11 April 2009
Received in revised form 13 May 2010
Accepted 14 May 2010

Keywords:
Convective heat transfer
Finite volume
Backward-facing step
Lattice Boltzmann
Double distribution function
Laminar flow

ABSTRACT

In this paper, Thermal Finite-Volume Lattice Boltzmann Method is developed. To demonstrate the temperature field, the Double Distribution Function (DDF) of thermal lattice Boltzmann equation is used. The upwind biasing factors based on pressure and temperature are defined and applied as flux corrector in the thermo-hydrodynamic lattice Boltzmann equations. A consistent open and solid boundary treatment of flow is also addressed. The unknown energy distribution at the boundary cells are decomposed into its equilibrium and non-equilibrium parts. Then the non-equilibrium part is approximated with extrapolation of the non-equilibrium part of the populations at the neighboring nodes. This treatment enlarges the domain stability and led up to faster convergence. Two test cases namely, thermo-hydrodynamic in a backward-facing step and around a circular cylinder inserted within a backward-facing step are carried out. The results are compared with the available solutions in the technical literature.

1. Introduction

Although in recent years, for incompressible isothermal flows, the Lattice Boltzmann Method (LBM) has been found to be at least as stable, accurate and computationally efficient, it is still a challenging problem to construct the thermo-hydrodynamic for a wide range of temperature variation through a robust numerical performance. The existing Lattice Boltzmann models for thermal flows in the literature fall into three categories, i.e., the passive-scalar approach, the multispeed approach and the DDF approach. The passive-scalar approach utilizes the fact that the macroscopic temperature satisfies the same evolution equation as a passive scalar if the viscous heat dissipation and compression work done by the pressure are negligible [1,2]. Extensive studies of two- and three-dimension Rayleigh–Benard convections using this method were made by Shan [3]. The multispeed models are an extension of the lattice Bhatnagar–Gross–Krook (LBGK) models for isothermal flows, in which only the single-particle distribution function is defined and a higher order of velocity moment of this distribution function is used to describe the temperature field. The main disadvantage of the multispeed LBGK models is that they usually suffer from serious numerical instability and is only suitable for problems with restricted temperature range [4]. In addition, the multispeed LBGK models using a single relaxation time are limited to problems with a fixed Prandtl number, which has no engineering applications. Although some methods have been proposed to cure these problems, the drawbacks of the multispeed models still limit their practical usage. Alternatively, the DDF models utilize an additional distribution function, instead of the original single-particle distribution function, to describe the evolution of the temperature field [5,6]. Moreover, the DDF models have better numerical stability than the multispeed models.

* Corresponding author. Tel.: +98 411 3392480; fax: +98 411 3354153.
E-mail addresses: ghasemi.j@znu.ac.ir, jghasemi@tabrizu.ac.ir, jalal_ghasemi@yahoo.com (J. Ghasemi).

0898-1221/$ – see front matter © 2010 Elsevier Ltd. All rights reserved.
doi:10.1016/j.camwa.2010.05.011

Although the lattice Boltzmann equation has been discretized by the finite-volume method on arbitrary mesh for different schemes in hydrodynamic solution [7–10] however, there is not yet any published work of the finite-volume combined with the thermal lattice Boltzmann equation. Hence, in this paper, a novel approach of combining DDF applied without the viscous heat dissipation and compression work terms with a cell-centered finite-volume method is presented which has several features. Of them, combining the finite volumes with the DDF and upwind biasing factors in both the momentum and thermal convective fluxes have been carried out. Applying these factors made it possible to overcome the main shortcoming of thermal lattice Boltzmann i.e., instability thereby accelerating the convergence process.

The implementation of thermal boundary conditions is a major step in thermal LBM. In [2], the bounce-back rule of the non-equilibrium distribution proposed by Zou and He [11] is applied to the thermal population. D'Orazio and Succi [12] assumed that the unknown thermal distribution functions at the boundary would be the equilibrium distribution functions, with a counter-slip internal energy density. This method is easy in implementation and is of the highest accuracy because it can guarantee the fixed velocity and temperature or heat flux at the wall exactly. Guo et al. [13] were first introduced the idea of decomposing energy distribution population at the boundary cells into the equilibrium and non-equilibrium parts and extended it in curved boundaries [14–17]. In present work, the explained boundary method coupled with the cell-centered finite-volume method which improved the computational efficiency. To implement the above mentioned ideas on in-house FORTRAN 90 code was written and developed by the authors.

2. Thermal finite-volume lattice Boltzmann method

The thermal lattice Boltzmann model involves two evolution equations. The compact discretized integral form along with simplified model [18] reads

$$\int_S \left(\frac{\partial \Re_i}{\partial t} + v_i.\nabla \Re_i + \frac{1}{\tau_\sigma}(\Re_i - \Re_i^{\mathrm{eq}}) \right) \mathrm{d}s = 0 \quad i = 0, 1, \ldots, M$$
$$\Re = f, g; \qquad \Re_i^{\mathrm{eq}} = f^{\mathrm{eq}}, g^{\mathrm{eq}}; \qquad \sigma = \nu, \mathrm{th} \tag{1}$$

where f and g are the particle and energy distribution functions, v_i shows the particle microscopic velocity in the ith direction. The f^{eq} and g^{eq} denote the equilibrium of particles and energy distribution functions. Also τ_ν and τ_{th} show the density and thermal relaxation times. In the D_2Q_9 lattice one has,

$$v_0 = 0; \qquad v_i = \left(\cos\left(\frac{i-1}{2}\pi\right), \sin\left(\frac{i-1}{2}\pi\right) \right) c, \quad i = 1, 2, 3, 4;$$
$$v_i = \sqrt{2}\left(\cos\left(\frac{i-5}{2} + \frac{1}{4}\right)\pi, \sin\left(\frac{i-5}{2} + \frac{1}{4}\right)\pi \right) c, \quad i = 5, 6, 7, 8; \tag{2}$$
$$c^2 = \frac{3k_B T}{m_p}$$

where $k_B = 1.38 \times 10^{-23}$ (N m K^{-1}) is the Boltzmann constant and T and m_p are temperature and particle mass, respectively. A cell-centered finite volume on arbitrary cells is shown in Fig. 1. According to Fig. 1, one gets

$$\int_{abcd} \frac{\partial \Re_i}{\partial t} \mathrm{d}s \approx \left[\frac{\partial \Re_i}{\partial t} \right]_{I,J} .S_{I,J} \tag{3}$$

and

$$\int_{abcd} v_i.\nabla \Re_i \, \mathrm{d}s = \int_{abcd} \left\{ \frac{\partial (v_{ix}.\Re_i)}{\partial x} + \frac{\partial (v_{iy}.\Re_i)}{\partial y} \right\} \mathrm{d}x \, \mathrm{d}y \approx \sum_k v_i.N_k[\tilde{\Re}_i]_k \tag{4}$$

where

$$N_k = (\Delta yi - \Delta xj)_k, \quad k = ab, bc, cd, da. \tag{5}$$

Here, the pressure- and temperature-based biasing factors in convective fluxes of Eq. (1) are employed as

$$\begin{aligned}
\xi^\sigma_{ab-L} &= \frac{\psi_{I-1,J}}{\psi_{I-1,J} + \psi_{I,J}}, & \xi^\sigma_{ab-R} &= \frac{\psi_{I,J}}{\psi_{I,J} + \psi_{I+1,J}} & \xi^\sigma_{ab} &= \frac{\xi^\sigma_{ab-L} + \xi^\sigma_{ab-R}}{2} \\
\xi^\sigma_{bc-B} &= \frac{\psi_{I,J-1}}{\psi_{I,J} + \psi_{I,J-1}}, & \xi^\sigma_{bc-T} &= \frac{\psi_{I,J}}{\psi_{I,J+1} + \psi_{I,J}} & \xi^\sigma_{bc} &= \frac{\xi^\sigma_{bc-B} + \xi^\sigma_{bc-T}}{2} \\
\xi^\sigma_{cd-R} &= \frac{\psi_{I+1,J}}{\psi_{I,J} + \psi_{I+1,J}}, & \xi^\sigma_{cd-L} &= \frac{\psi_{I,J}}{\psi_{I,J} + \psi_{I-1,J}} & \xi^\sigma_{cd} &= \frac{\xi^\sigma_{cd-R} + \xi^\sigma_{cd-L}}{2} \\
\xi^\sigma_{da-T} &= \frac{\psi_{I,J}}{\psi_{I,J} + \psi_{I,J+1}}, & \xi^\sigma_{da-B} &= \frac{\psi_{I,J}}{\psi_{I,J} + \psi_{I,J-1}} & \xi^\sigma_{da} &= \frac{\xi^\sigma_{da-T} + \xi^\sigma_{da-B}}{2}
\end{aligned} \tag{6}$$

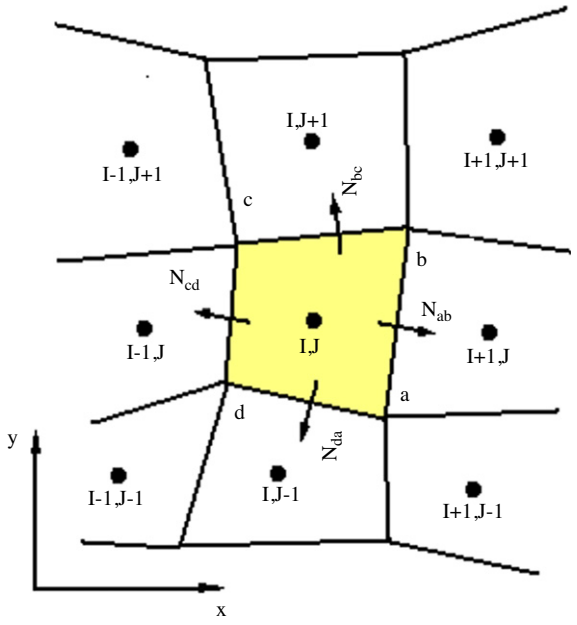

Fig. 1. Cell-centered finite volumes.

where, ψ takes the p and T for pressure and temperature, respectively. The convective fluxes are approximated as following:

$$\int_{abcd} v_i.\nabla\Re_i \,\mathrm{d}s \approx \left\{ v_i.N_{ab}(\xi^{\sigma}_{ab}[\Re_i]_{I,J} + (1-\xi^{\sigma}_{ab})[\Re_i]_{I+1,J}) + v_i.N_{bc}(\xi^{\sigma}_{bc}[\Re_i]_{I,J} + (1-\xi^{\sigma}_{bc})[\Re_i]_{I,J+1}) \right.$$
$$\left. + \; v_i.N_{cd}(\xi^{\sigma}_{cd}[\Re_i]_{I,J} + (1-\xi^{\sigma}_{cd})[\Re_i]_{I-1,J}) + v_i.N_{da}(\xi^{\sigma}_{da}[\Re_i]_{I,J} + (1-\xi^{\sigma}_{da})[\Re_i]_{I,J-1}) \right\}. \tag{7}$$

By linear approximation of $\Re_i$, $\Re^{\mathrm{eq}}_i$ over each internal cell in Fig. 1, the integration of the collision terms in Eq. (1) becomes

$$-\int_{abcd} \frac{1}{\tau_\sigma}(\Re_i - \Re^{\mathrm{eq}}_i)\mathrm{d}s = -\frac{S_{I,J}}{\tau_\sigma}\left[\frac{1}{4}[\Delta\Re_i]_{I,J} + \frac{1}{8}\left\{[\Delta\Re_i]_{I+1,J} + [\Delta\Re_i]_{I,J+1} + [\Delta\Re_i]_{I-1,J} + [\Delta\Re_i]_{I,J-1}\right\}\right.$$
$$\left. + \frac{1}{16}\left\{[\Delta\Re_i]_{I+1,J-1} + [\Delta\Re_i]_{I+1,J+1} + [\Delta\Re_i]_{I-1,J+1} + [\Delta\Re_i]_{I-1,J-1}\right\}\right] \tag{8a}$$

and in boundary cells it takes the following form

$$-\int_{abcd} \frac{1}{\tau_\sigma}(\Re_i - \Re^{\mathrm{eq}}_i)\mathrm{d}s = -\frac{S_{I,J}}{\tau_\sigma}[[\Re_i]_{I,J} - [\Re^{\mathrm{eq}}_i]_{I,J}] \tag{8b}$$

where $S_{I,J}$ is the cell area and

$$\Delta\Re_i = \Re_i - \Re^{\mathrm{eq}}_i. \tag{9}$$

In flux averaging, the addition of artificial dissipation is inevitable to damp out the spurious oscillations. It is taken as

$$[D^{(4)}\Re_i]_{I,J} = \varepsilon^{\sigma}_x.(\nabla\Delta)^2_x.[\Re_i]_{I,J} + \varepsilon^{\sigma}_y.(\nabla\Delta)^2_y.[\Re_i]_{I,J} \tag{10}$$

where ε^{σ}_x and ε^{σ}_y are used in thermo-hydrodynamic equations. The integration over each cell is the sum of contributed terms. The $\Re_i$ is updated by modified fifth-order Runge–Kutta schemes follows

$$\begin{aligned}
&\Re^{n+1} = \Re^n + \alpha_k \Delta\Re^{k-1}; \quad k = 1,\ldots,5;\\
&\alpha_1 = 0.0695, \quad \alpha_2 = 0.1602, \quad \alpha_3 = 0.2898, \quad \alpha_4 = 0.5, \quad \alpha_5 = 1;\\
&\Delta\Re^{k-1} = \frac{\Delta t}{S_{I,J}} Q^{k-1}; \quad Q^{k-1} = \sum[\Re^{k-1}]_{\mathrm{Collisions}} - \sum[\Re^{k-1}]_{\mathrm{Fluxes}}
\end{aligned} \tag{11}$$

where n denotes the time level, *Collisions* and *Fluxes* refer to collision and flux terms. The particle equilibrium function, $\Re_i^{eq} = f_i^{eq}$, is given by [2,18]:

$$\begin{aligned} f_0^{eq} &= \frac{4}{9}\rho\left[1 - \frac{3}{2c^2}\mathbf{u}.\mathbf{u}\right]; \\ f_{1,2,3,4}^{eq} &= \frac{1}{9}\rho\left[1 + \frac{3}{c^2}v_i.\mathbf{u} + \frac{9}{2c^4}(v_i.\mathbf{u})^2 - \frac{3}{2c^2}\mathbf{u}.\mathbf{u}\right] \\ f_{5,6,7,8}^{eq} &= \frac{1}{36}\rho\left[1 + \frac{3}{c^2}v_i.\mathbf{u} + \frac{9}{2c^4}(v_i.\mathbf{u})^2 - \frac{3}{2c^2}\mathbf{u}.\mathbf{u}\right] \end{aligned} \tag{12a}$$

and the energy equilibrium function, $\Re_i^{eq} = g_i^{eq}$, is given by [2,18]

$$\begin{aligned} g_0^{eq} &= -\frac{2\rho\varepsilon}{3}\frac{\mathbf{u}^2}{c^2} \\ g_{1,2,3,4}^{eq} &= \frac{\rho\varepsilon}{9}\left[\frac{3}{2} + \frac{3}{2c^2}v_i.\mathbf{u} + \frac{9}{2c^4}(v_i.\mathbf{u})^2 - \frac{3}{2c^2}\mathbf{u}.\mathbf{u}\right] \\ g_{5,6,7,8}^{eq} &= \frac{\rho\varepsilon}{36}\left[3 + \frac{6}{c^2}v_i.\mathbf{u} + \frac{9}{2c^4}(v_i.\mathbf{u})^2 - \frac{3}{2c^2}\mathbf{u}.\mathbf{u}\right] \end{aligned} \tag{12b}$$

where $\varepsilon = \mathrm{DRT}/2$ (D is the dimension and R is the gas constant). Then the macroscopic density, velocity and temperature are calculated as

$$\rho = \sum_{i=0}^{8} f_i, \qquad \rho\mathbf{u} = \sum_{i=0}^{8} v_i f_i, \qquad \rho\varepsilon = \sum_{i=0}^{8} g_i. \tag{13}$$

The Chapman–Enskog expansion for the density distribution function can recover the continuity, Navier–Stokes and energy equations. The detailed derivation can be found in [2,12,19] and will not be shown here. The pressure is given by the equation of state of an ideal gas as

$$p = c_s^2\rho, \qquad c_s = \frac{c}{\sqrt{3}}. \tag{14}$$

Here, c_s is the speed of sound. The kinematic viscosity, υ and the thermal diffusivity, α are determined by [20]

$$\upsilon = \left(\frac{2\tau_\upsilon - 1}{6}\right)\frac{(\Delta x)^2}{\Delta t}; \qquad \alpha = \frac{2}{3}\left(\tau_e - \frac{1}{2}\right)\Delta t. \tag{15}$$

It is consistent for both Navier–Stokes and energy equation provided viscous heating effect and compression work done by the pressure are negligible. The Prandtl number becomes

$$\mathrm{Pr} = \frac{\tau_\upsilon - 1/2}{2\tau_e - 1}\Delta x^2. \tag{16}$$

The local Nusselt number is defined as [17]

$$Nu_x = \frac{D_h q_{w,x}}{\kappa}.\frac{1}{(T_{w,x} - T_{\mathrm{bulk},x})} \tag{17}$$

where D_h is the hydraulic diameter, $q_{w,x} = \kappa(\partial T_w/\partial n)$ is the solid wall local heat flux and $T_{\mathrm{bulk},x} = \int \rho.\mathbf{u}.T\,\mathrm{d}\mathbf{n}/\int \rho.\mathbf{u}\mathrm{d}\mathbf{n}$ is the bulk temperature in $\mathbf{x}$ location section.

The time step is computed based on the following

$$\Delta t = \frac{\mathrm{CFL} * \mathrm{Min}\left(\sqrt{\Delta x_{I,J}^2 + \Delta y_{I,J}^2}\right)}{\mathrm{Max}\left(\sqrt{u_{I,J}^2 + v_{I,J}^2}\right)}. \tag{18}$$

Residuals, Res_υ and $\mathrm{Res}_{\mathrm{th}}$ of the velocity and temperature convergence criterion are set to

$$\mathrm{Res}_\upsilon = \frac{\sum_{I,J}\left|\sqrt{(u_{I,J}^2 + v_{I,J}^2)^{n+1}} - \sqrt{(u_{I,J}^2 + v_{I,J}^2)^n}\right|}{\sum_{I,J}\left|\sqrt{(u_{I,J}^2 + v_{I,J}^2)^n}\right|}; \qquad \mathrm{Res}_{\mathrm{th}} = \frac{\sqrt{\sum_{I,J}\left|T_{I,J}^{n+1} - T_{I,J}^n\right|^2}}{\sqrt{\sum_{I,J}\left|T_{I,J}^n\right|^2}}. \tag{19}$$

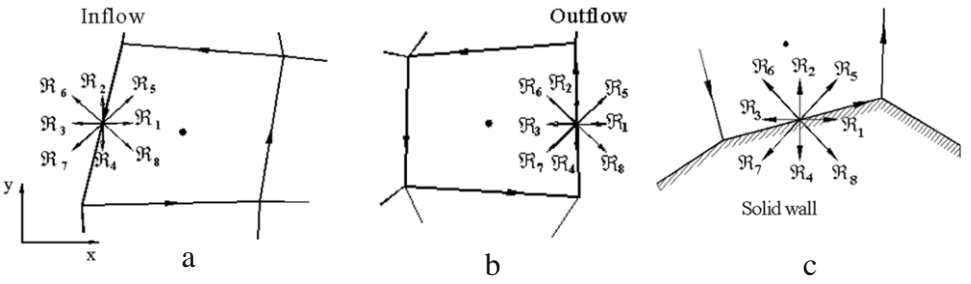

Fig. 2. Typical boundary cells: (a) inflow, (b) outflow, (c) solid wall.

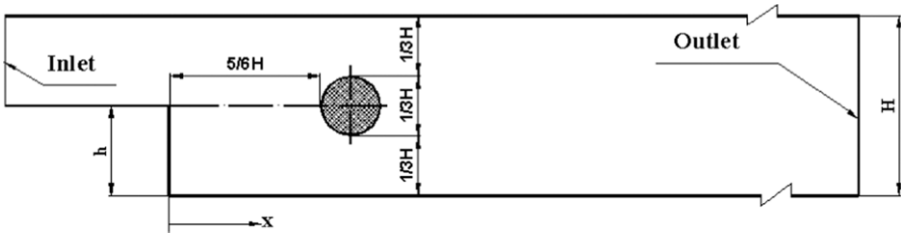

Fig. 3. Configuration of the backward-facing step with a cylinder.

3. Velocity and thermal boundary conditions

In practical applications, the flow boundary conditions are usually specified in terms of the fluid variables. In order to transform thermo-hydrodynamic boundary conditions to the boundary conditions for the distribution functions, we employ the additional D_2Q_9 lattices at the edge of each cell of inflow, outflow and solid boundaries, as shown in Fig. 2(a), (b) and (c), respectively. The implementation of velocity boundary conditions is consistent based on characteristics [21,22] of hydraulic Boltzmann equation [23]. For the thermal boundary conditions, a consistent open and solid boundary treatment of flow is also used. The unknown energy distribution population at the boundary cells are decomposed into its equilibrium and non-equilibrium parts [16]. The non-equilibrium part is approximated with a first-order extrapolation of the non-equilibrium part of the populations at the neighboring cells. Then the, g_i, at the node of boundary cell can be determined as

$$g_i(x_b) = g_i^{\mathrm{eq}}(x_b, \rho_b, \varepsilon_b) + [g_i(x_f) - g_i^{\mathrm{eq}}(x_f, \rho_f, \varepsilon_f)] \tag{20}$$

where subscripts b and f denoted the boundary cell and nearest neighboring cell to the boundary cell, respectively. A good approximation for unknown ρ_b in boundary cells is ρ_f. For the Dirichlet type condition, the given temperature by energy distribution function, based on Eq. (20), is applied directly on the boundary. The Neumann type condition is transferred to the Dirichlet type condition through the conventional second-order finite difference approximation in order to obtain the temperature at the boundary [24].

4. Numerical results

In order to validate the method presented in this paper, three specified test cases is considered. The geometry of physical domain is shown in Fig. 3. Hence, the thermo-hydrodynamic modeling is considered as following:

Case 1: For the backward-facing step with $H = 3h$, the hydrodynamic boundary condition are the same as Razavi et al. [23]. However, for the thermal boundary conditions only the lower wall after the step is kept at constant temperature and all the others are treated as adiabatic.

Case 2: In the backward-facing step with $H = 2h$, the hydrodynamic boundary conditions are similar to the Case 1. Unlike the Case 1 all the walls are kept at constant temperature lower than the inlet constant temperature.

Case 3: In the backward-facing step with $H = 2h$, including a cylindrical obstacle, the flow and thermal boundary conditions are the same as Case 1 for backward-facing step. In addition, the cylindrical obstacle is assumed to be adiabatic.

The Reynolds number (Re) of the flow for all cases as $4U(H-h)/3\nu$, where U is the maximum velocity in the inlet.

4.1. Influence of the pressure- and temperature-biasing factors

Initially, we investigate the performance of the pressure- and temperature-biasing factors in our numerical solution. A survey of pressure-biasing factors can be found in [23]. This was led to an improvement in the stability and accuracy of numerical scheme and reduced the iteration steps. Also, the results of Fig. 4 show the residuals of temperature with and

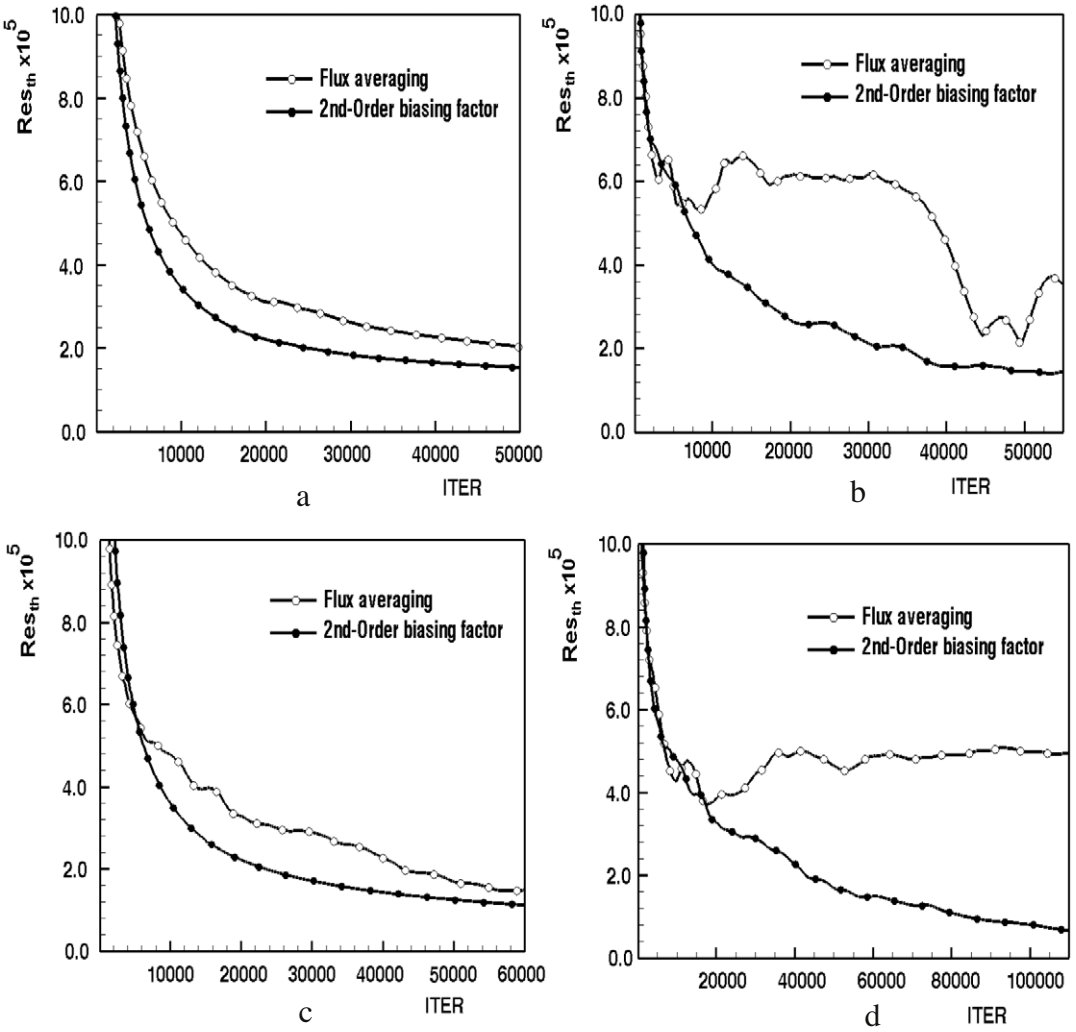

Fig. 4. Influence of temperature-based biasing factor in numerical accuracy and convergence, case 3: (a) $Re = 20$, (b) $Re = 50$, (c) $Re = 80$, (d) $Re = 200$; cases (a) and (b) without dissipation, cases (c) and (d) with minimum dissipation.

without applying these factors for thermal equation in Case 3 at $Re = 20, 50, 80, 200$. As it is seen, applying the temperature-biasing factors increases the stability and enabled us to get steady solutions in a wide range of Reynolds numbers. This factor was applied without adding any artificial dissipation for $Re = 20, 50$ and the minimal artificial dissipation for $Re = 80, 200$. Hence a better convergence was achieved for second-order temperature-biasing factor. Applying the temperature-biasing factor enabled us to overcome to some shortcomings, specially, numerical instability of thermal lattice Boltzmann formulations. All the next calculations are based on the same flux model.

4.2. Results of thermo-fluid behavior

The backward-facing step was used as a benchmark for numerical and experimental hydrodynamics [25–31] and thermal [20,32,33]. Fig. 3 shows the configuration of the physical domain (without cylindrical obstacle). At the inlet boundary, the velocity is taken as fully developed and the temperature is constant. The outlet boundary was set far enough from the step that we could impose Neumann conditions for velocity and temperature. Grid (lattice) independence for non-dimensionalized reattachment length (L_1/H) was shown at $Re = 50$ in Fig. 5 for Case 1 (L_1 shown in Fig. 6). According to Fig. 5, a 1064×64 mesh size was chosen. Fig. 6 show the typical streamlines and L_1, L_2, L_3 reattachment lengths. Table 1 demonstrates a summary of quantitative results for non-dimensionalized reattachment lengths $\left(\frac{L_1}{h}, \frac{L_2}{h}, \frac{L_3}{h}\right)$ compared to the present work. Fig. 7(a) shows the distribution of local Nu versus Re for Case 1. The results depict that as the $\frac{x}{h}$ ratio increases the value of Nu rises up within this region and then falls down. Also, it can be observed that with increasing the Re, the peak value of Nu not only increases, but also moves downstream of the domain. This movement of the peak

Table 1
The comparison of the non-dimensionalized reattachment lengths (a) Case 1, (b) Case 2.

(a)			
Re	$\frac{L_1}{h}$		
	40	*73*	*229*
Denham et al. [25][a]	2.71	3.89	9.89
Barber et al. [26][a]	2.53	3.64	9.75
Present study	***2.485***	***3.710***	***9.527***

(b)							
Re	$\frac{L_1}{h}$			$\frac{L_2}{h}$		$\frac{L_3}{h}$	
	100	*150*	*200*	*400*	*450*	*400*	*450*
Armaly et al. [27][b]	–	4.04	5.13	7.35	7.15	–	9.89
Guj et al. [29][a]	2.91	–	4.81	–	–	–	–
Barton [30][a]	–	3.85	4.87	7.32	7.96	9.32	10.34
Erturk [31][a]	2.95	–	4.96	7.65	–	9.85	–
Present study	***2.964***	***4.154***	***4.876***	***6.824***	***6.936***	***9.453***	***10.863***

[a] Numerical.
[b] Experimental.

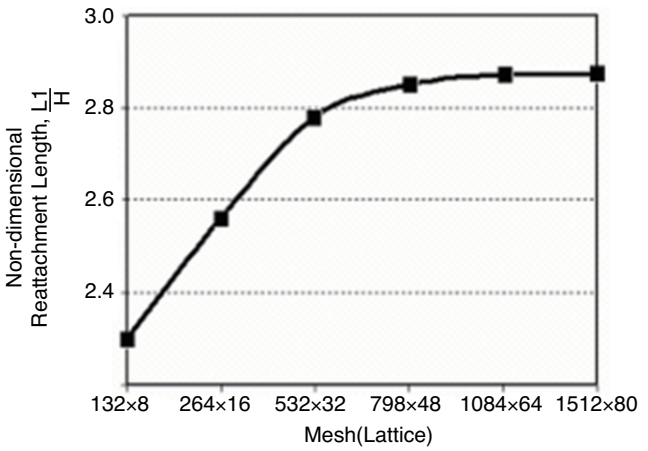

Fig. 5. Reattachment length (L_1/H) versus mesh (lattice) numbers.

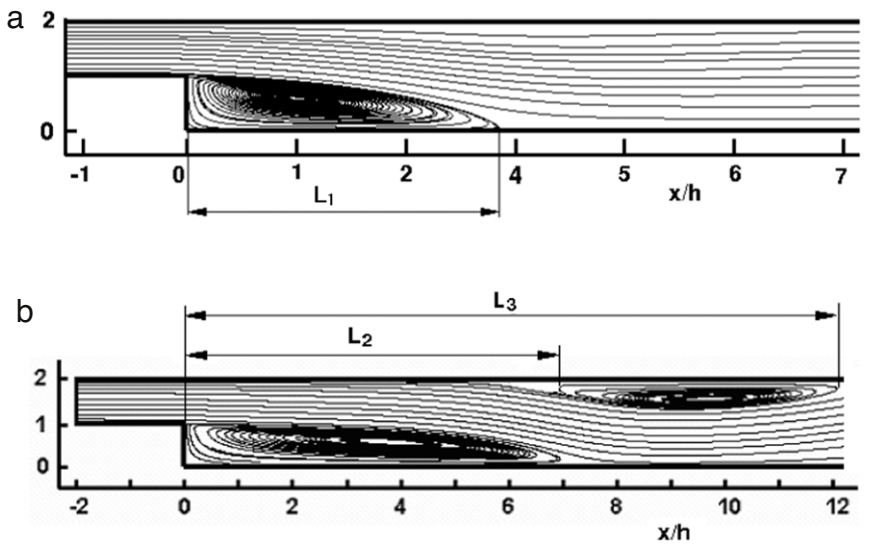

Fig. 6. Typical streamlines, case 2: (a) $Re = 145$, (b) $Re = 485$.

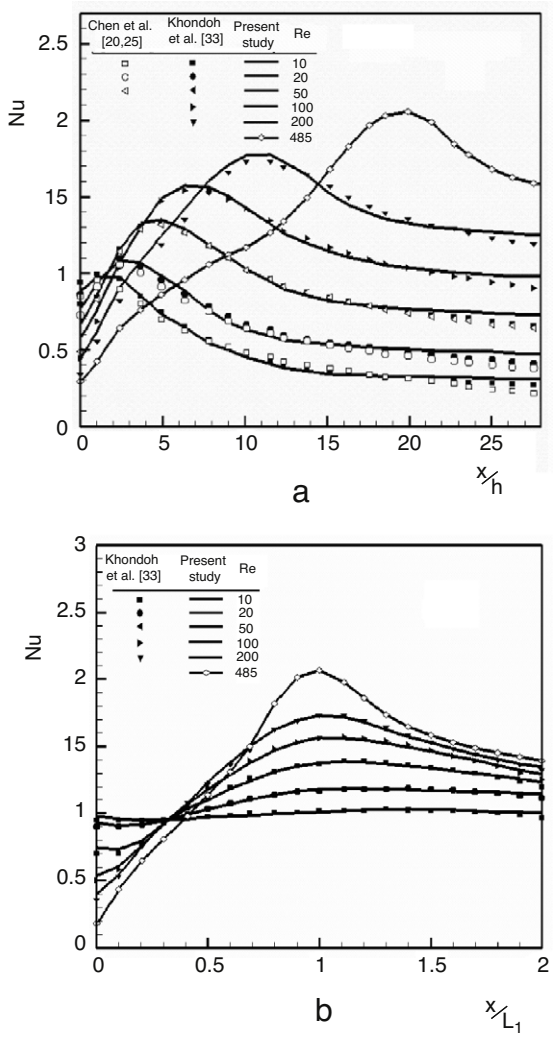

Fig. 7. Local *Nu* versus Reynolds number, case 1: Pr = 0.7 (a) *Nu* versus $\frac{x}{h}$, *Nu* versus $\frac{x}{L_1}$.

values of *Nu* seems to be related to the movement of the flow reattachment point. Thus, *Nu* is replotted in Fig. 7(b) with the abscissa, *x*, normalized by the reattachment length, L_1. This result reveals that the peak value of *Nu* is approximately located in reattachment point. Moreover, the present solutions have reasonable agreement with the numerical results of Refs. [20,32,33]. Fig. 8 expresses the influence of the *Re* on the local *Nu* distribution of the lower heat exchanging wall for Case 2. The trend of solutions follow a certain pattern in Case 1 (Fig. 7(a)), however, the results obtained for the *Nu* curves and values are somewhat different based on the corresponding thermal boundary conditions. Besides, the peak values of *Nu* still related to Reynolds numbers and movement of the reattachment length. A good agreement exists between our numerical results and that of Refs. [25–31].

Fig. 9 shows the typical streamlines of velocity field at $Re = 150$ for Case 3. For the same case, Fig. 10 shows the influence of the *Re* on the local *Nu* distribution. It can be noticed that the local *Nu* values are higher than in the case without cylindrical obstacle. In other words, by inserting the cylindrical obstacle the flow streamlines are dislocated and shifts the location of reattachment point (L_1) towards the step. Also, it changed the velocity field and influences the thermal boundary layer. Therefore, the presence of cylinder could affect both the hydrodynamics and thermal flow behavior. Commonly, this makes an enhancement in heat transfer process and this enhancing effect is seen particularly at higher Reynolds numbers. Also the results are in favorable agreement with other numerical solutions [32].

5. Conclusions

In this paper the D_2Q_9 lattice coincided with non-uniform grids is used by combining a cell-centered finite volume and DDF of thermal lattice Boltzmann method. A novel approach is proposed for the convective flux treatment of thermo-

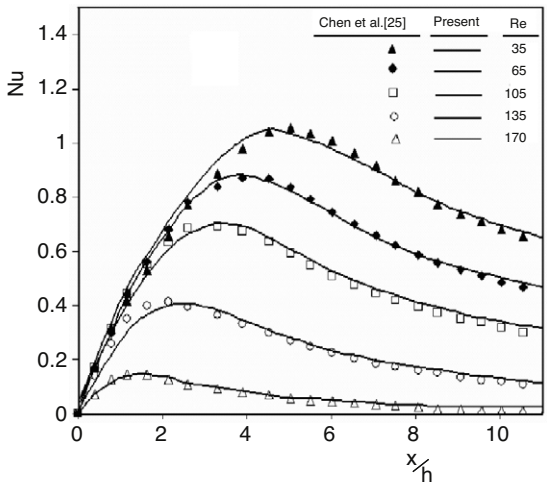

Fig. 8. Local *Nu* versus *Re*, case 2: Pr = 0.7.

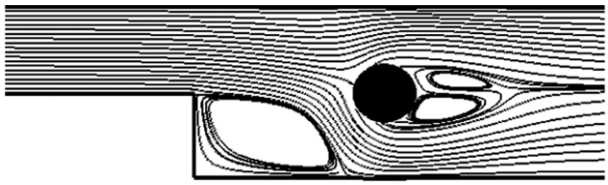

Fig. 9. Typical streamlines with cylindrical obstacle, case 3: *Re* = 150.

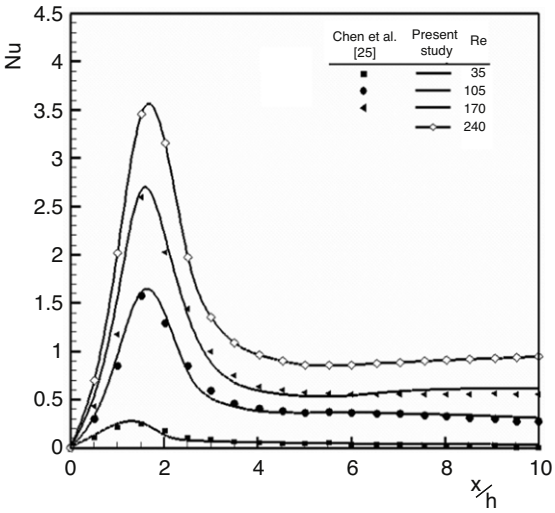

Fig. 10. Local *Nu* versus *Re*, case 3: Pr = 0.7.

hydrodynamic lattice Boltzmann, which takes into account the second-order pressure- and temperature-based biasing factors. These factors make the scheme to be dominantly upwinded. This approach successfully broadened the numerical stability region and improved accuracy of solutions for both the velocity and temperature fields and reduced the convergence steps. Applying the temperature-biasing factor enabled the scheme to compensate some shortcomings, specially, the numerical instability of thermal lattice Boltzmann formulations. Optimal boundary conditions, the decomposition of energy distribution population at the boundary cells into equilibrium and non-equilibrium parts, were successfully applied. This raised the accuracy of thermo-hydrodynamic results and well applicable to cell-centered thermal finite-volume lattice Boltzmann in complex geometries.

References

[1] F. Massaioli, R. Benzi, S. Succi, Exponential tails in two-dimensional Rayleigh–Bénard convection, Europhys. Lett. 21 (1993) 305–310.
[2] X. He, S. Chen, G.D. Doolen, A novel thermal model for the lattice Boltzmann method in incompressible limit, J. Comput. Phys. 146 (1998) 282–300.
[3] X. Shan, Solution of Rayleigh–Benard convection using a lattice Boltzmann method, Phys. Rev. E 55 (1997) 2780–2788.
[4] Y. Shi, T.S. Zhao, Z.L. Guo, Thermal lattice Bhatnagar–Gross–Krook model for flows with viscous heat dissipation in the incompressible limit, Phys. Rev. E 70 (2004) Art. No. 066310.
[5] R.G.M. Van der Sman, Lattice Boltzmann scheme for natural convection in Porous media, Internat. J. Modern Phys. C 8 (1997) 879–888.
[6] B.J. Palmer, D.R. Rector, Lattice Boltzmann algorithm for simulating thermal flow in compressible fluids, J. Comput. Phys. 161 (2000) 1–20.
[7] F. Nannelli, S. Succi, The lattice Boltzmann equation in irregular lattices, J. Stat. Phys. 68 (3–4) (1992) 401–407.
[8] H. Xi, G. Peng, S. Chou, Finite-volume lattice Boltzmann method, Phys. Rev. E 59 (1999) 6202–6205.
[9] S. Ubertini, S. Succi, Recent advances of lattice Boltzmann techniques on unstructured grids, Prog. Comput. Fluid Dyn. 5 (2005) 85–96.
[10] M. Stiebler, J. Tolke, M. Krafczyk, An upwind discretization scheme for the finite volume lattice Boltzamnn method, Comput. Fluids 35 (2006) 814–819.
[11] Q. Zou, X. He, On pressure and velocity boundary conditions for the lattice Boltzmann BGK model, Phys. Fluids 9 (6) (1997) 1591–1598.
[12] A. D'Orazio, S. Succi, Simulating two-dimensional thermal channel flows by means of a lattice Boltzmann method with new boundary conditions, Future Gener. Comput. Syst. 20 (2004) 935–944.
[13] Z.L. Guo, C. Zheng, B. Shi, An extrapolation method for boundary conditions in lattice Boltzmann method, Phys. Fluids 14 (2002) 2007–2010.
[14] A. D'Orazio, M. Corcione, G.P. Celata, Application to natural convection enclosed flows of a lattice Boltzmann BGK model coupled with a general purpose thermal boundary condition, Int. J. Therm. Sci. 43 (2004) 575–586.
[15] Z.L. Guo, B. Shi, C. Zheng, A coupled lattice BGK model for the Boussinesq equations, Internat. J. Numer. Methods Fluids 39 (2002) 325–342.
[16] Z.L. Guo, C. Zheng, B. Shi, Thermal lattice Boltzmann equation for low mach number flows: decoupling model, Phys. Rev. E 75 (2007) Art. No. 036704.
[17] G.H. Tang, W.Q. Tao, Y.L. He, Thermal boundary condition for the thermal lattice Boltzmann equation, Phys. Rev. E 72 (2005) Art. No. 016703.
[18] Y. Peng, C. Shu, Y.T. Chew, Simplified thermal lattice Boltzmann model for incompressible thermal flows, Phys. Rev. E 68 (2003) Art. No. 026701.
[19] S. Succi, The Lattice Boltzmann Equation for Fluid Dynamics and Beyond, Oxford University Press Inc., New York, 2001.
[20] C.K. Chen, T.S. Yen, Y.T. Yang, Lattice Boltzmann method simulation of backward-facing step on convective heat transfer with field synergy principle, Int. J. Heat Mass Transfer 49 (2006) 1195–1204.
[21] S.E. Razavi, K. Zamzamian, A. Farzadi, Genuinely multidimensional characteristic-based scheme for incompressible flows, Internat. J. Numer. Method Fluids 57 (8) (2008) 929–949.
[22] K. Zamzamian, S.E. Razavi, Multidimensional upwinding for incompressible flows based on characteristics, J. Comput. Phys. 227 (2008) 8699–8713.
[23] S.E. Razavi, J. Ghasemi, A. Farzadi, Flux modeling in the finite-volume lattice Boltzmann approach, Int. J. Comput. Fluid Dyn. 23 (1) (2009) 69–77.
[24] C. Shu, Y. Peng, Y.T. Chew, Simulation of natural convection in a square cavity by Taylor series expansion and least square-based lattice Boltzmann method, Internat. J. Modern Phys. C 13 (2002) 1399–1414.
[25] M.K. Denham, M.A. Patrick, Laminar flow over a downstream-facing step in a two dimensional flow channel, Trans. Inst. Chem. Eng. 52 (1974) 361–367.
[26] R.W. Barber, A. Fonty, A numerical study of laminar flow over a confined backward-facing step using a novel viscous-splitting vortex algorithm, in: 4th GRACM Congress on Comput. Mech., 2002.
[27] B.F. Armaly, F. Durst, J.C.F. Pereira, B. Schonung, Experimental and theoretical investigation of backward-facing step flow, J. Fluid Mech. 127 (1983) 473–496.
[28] A.F. Ghoniem, Y. Gagnon, Vortex simulation of laminar recirculating flow, J. Comput. Phys. 68 (1987) 346–377.
[29] G. Guj, F. Stella, Numerical solutions of high-Re recirculating flows in vorticity-velocity form, Internat. J. Numer. Methods Fluids 8 (1988) 405–416.
[30] I.E. Barton, A numerical study of flow over a confined backward-facing step, Internat. J. Numer. Methods Fluids 21 (1995) 653–665.
[31] E. Erturk, Numerical solutions of 2-d steady incompressible flow over a backward-facing step, part I: high Reynolds number solutions, Int. J. Comput. Fluid Dyn. 37 (2008) 633–655.
[32] C.K. Chen, T.S. Yen, Y.T. Yang, Lattice Boltzmann method of a cylinder in the backward-facing step with field synergy principle, Int. J. Therm. Sci. 45 (2006) 982–989.
[33] T. Kondoh, Y. Nagano, T. Tsuji, Computational study of laminar heat transfer downstream of a backward-facing step, Int. J. Heat Mass Transfer 36 (1993) 577–591.